decreased in both distilled water and PBS. The dispersibility of water-soluble H-CNFs was higher in distilled water than PBS. Sedimentation is related to the ratio of the amount of hydrophilic group per surface area, their own weight and length, and the critical coagulation concentration (*ccc*) of the hydrophilic-modified carbon nanotubes.

ACKNOWLEDGMENTS

This work was supported by a Grant-in-Aid for Basic Research No. (S) 14103016 from the Ministry of Education, Science, Culture and Sport of Japan, Grant No. H18-chemistry-006 from Health and Labor Sciences Research Grants from the Ministry of Health, Labor and Welfare, Tohoku University 21st Century COE Program "International COE of Flow Dynamics", Arai Science and Technology Foundation, and the Collaborative Research facility from the Center for Interdisciplinary Research, Tohoku University.

REFERENCES

1. C. M. Says, J. D. Fortner, W. Guo, D. Lyon, A. M. Boyd, K. D. Ausman, Y. J. Tao, B. Sitharaman, L. J. Wilson, J. B. Hughes, J. L. West and V. L. Colvin, *Nano Lett.* **4**, 1881-1887 (2004).
2. D. B. Warheit, B. R. Laurence, K. L. Reed, D. H. Roach, G. A. M. Reynolds and T. R. Webb, *Toxicol. Sci.* **77**, 117-125 (2004).
3. C. W. Lam, J. T. James, R. McCluskey and R. L. Hunter, *Toxicol. Sci.* **77**, 126-134 (2004).
4. K. Kiura, Y. Sato, M. Yasuda, B. Fugetsu, F. Watari, K. Tohji and K. –I. Shibata, *J. Biomed. Nanotech.* **1**, 359-364 (2005).
5. Y. Sato, A. Yokoyama, K. –I. Shibata, Y. Akimoto, Y. Nodasaka, T. Kohgo, K. Tamura, T. Akasaka, M. Uo, K. Motomiya, B. Jeyadevan, M. Ishiguro, R. Hatakeyama, F. Watari and K. Tohji, *Mol. BioSyst.* **1**, 176-186 (2005).
6. S. Koyama, M. Endo, Y. –A. Kim, T. Hayashi, T. Yanagisawa, K. Osaka, H. Koyama, H. Haniu and N. Kuroiwa, *Carbon* **44**, 1079-1092 (2006).
7. H. Dumortier, S. Lacotte, G. Pastorin, R. Marega, W. Wu, D. Bonifazi, J.-P. Briand, M. Prato, S. Muller and A. Bianco, *Nano Lett.* **6**, 1522-1528 (2006).
8. J. C. Carrero-Sanchez, A. L. Elias, R. Mancilla, G. Arrellin, H. Terrones, J. P. Laclette and M. Terrones, *Nano Lett.* 6, 1609-1616 (2006).
9. A. Yokoyama, Y. Sato, Y. Nodasaka, S. Yamamoto, T. Kawasaki, M. Shindoh, T. Kohgo, T. Akasaka, M. Uo, F. Watari and K. Tohji, *Nano Lett.* **5**, 157-161 (2005).
10. N. M. Rodriguez, *J. Mater. Res.* **8**, 3233-3250 (1993).
11. M. Sano, J. Okamura and S. Shinkai, *Langmuir* **17**, 7172-7173 (2001).

Dental Materials Journal 26(2): 178−185, 2007

Carbon Nanotubes as Scaffolds for Cell Culture and Effect on Cellular Functions

Naofumi AOKI, Tsukasa AKASAKA, Fumio WATARI and Atsuro YOKOYAMA
Graduate School of Dental Medicine, Hokkaido University, Kita 13, Nishi 7, Kita-ku, Sapporo 060-8586, Japan
Corresponding author, Naofumi Aoki; E-mail: nao11@den.hokudai.ac.jp

Received October 11, 2006 /Accepted November 8, 2006

To investigate the dependence of biocompatibility of carbon materials on crystal structure with the aim of developing biomedical applications, single-(SW) and multi-walled (MW) carbon nanotubes (CNTs) were employed as scaffolds for cell culture and compared with graphite (GP). SaOS2 cells were used to investigate the properties and response of osteoblast-like cells. Polycarbonate membranes (PC) coated with CNTs by vacuum filtration formed a meshwork nanostructure. Cells grown on CNTs greatly extended in all directions. In terms of cell proliferation, alkaline phosphatase (ALP) activity, and protein adsorption on the substrates, CNTs showed better results than PC and GP. SW showed the best cell proliferation and total ALP. These favorable results might be attributed to the structure of CNTs and the affinity of CNTs toward proteins, thereby suggesting that CNTs could be potential scaffold materials for cell culture.

Keywords: Carbon nanotubes, Scaffold, Osteoblast

INTRODUCTION

In the imminent ageing society of the 21st century, nanotechnology[1,2] is a core technology to promoting health and improving QOL (quality of life) by enabling new health care technologies. In this connection, nanomaterials have been widely investigated for potential application in the medical field—ranging from making improved diagnostic methods to drug delivery systems, and from tissue regeneration to artificial prostheses[3,4]. In particular, carbon nanotubes (CNTs)—one of the most representative nanomaterials—were first reported by Iijima in 1991[5]. CNTs consist of carbon atoms and have unique electronic, catalytic, chemical, and mechanical properties[6]. Although CNTs have been widely studied, most of the studies focused on the physical, electrical, and chemical fields, with very few on biomedical applications[7-9].

Of late, there were reports on possible toxicity of CNTs[10-13], arising from their fibrous structure which resembles that of asbestos fibers causing lung cancer. Logically then, their safety as a biomaterial has been a matter of grave concern. Against this background, our previous *in vivo* and *in vitro* studies on nanocarbon materials investigated their possible use as a biomaterial. Yokoyama *et al.*[14] reported that hat-stacked carbon nanofibers did not cause a severe inflammatory response, and Wang *et al.*[15] reported that sintered bulk carbon nanotube materials exhibited sufficient biocompatibility. Moreover, Aoki *et al.*[16,17] reported on cell proliferation on multi-walled CNTs. Nonetheless, further investigations on cell functions such as enzymatic activity were deemed necessary to evaluate their biocompatibility for the development of biological applications.

The last decade has seen a dramatic development in biomedical technology, especially bone regeneration in tissue engineering. Scaffolds play a key role in most tissue engineering strategies[18,19]. In particular for bone bioengineering, one of the most important steps is to create scaffold materials that have the capacity to sustain bone cell growth and proliferation, as well as increment or replace bone tissue[20]. To date, scaffolds constructed with various materials such as porous polymers and ceramics have been reported[21,22]. Then recently, there have been several reports on the application of CNTs for scaffolds due in part to their unique mechanical, physical, and chemical properties[16,17,20,23]. For example, Mattson *et al.*[24] reported that CNTs coated with bioactive molecules were used as substrates for nerve cell growth. Webster *et al.*[25] reported that carbon nanofibers increased osteoblast functions. Similarly, MacDonald *et al.*[26] demonstrated that collagen-CNT composite materials could be used as scaffolds in tissue engineering.

CNTs come in two principal types: multi-walled (MW) and single-walled (SW). Due to their different crystal structures, these two types of CNTs show different electronic, catalytic, physical, and chemical properties. CNTs are also compared with graphite (GP). Both are isomorphs of pure carbon, composed of the same graphene sheet structure—where CNTs have the cylindrical structure, while GP have the layered sheet structure. However, there is scarce information about cellular response to the different crystal structures. The aim of the present study,

therefore, was to investigate the biological responses of cell proliferation and function on CNT scaffolds and their dependence on the crystal structures of MW and SW using osteoblast-like cells (SaOS2). These osteoblast cell responses were then compared with those of GP.

MATERIALS AND METHODS

Materials

MW carbon nanotubes of 5–20 nm in diameter and 20–40 μm in length synthesized by the chemical vapor deposition technique with purity of 98.17% (NanoLab Inc., MA, USA) were treated with hydrochloric acid to remove metal catalysts[27]. SW of 1.3–1.5 nm in diameter and 2–3 μm in length synthesized by arc discharge with purity of 99.56% (NanoLab Inc., MA, USA) were also treated in the same way. The GP particles used in this study were 4.5 μm in diameter.

Fabrication of scaffolds

CNTs and GP (200 μg) were dispersed in 100 mL of deionized water by sonication for 15 minutes. Then, scaffolds were made by vacuum filtration of the dispersed CNTs and GP slurry onto a porous polycarbonate membrane of 47 mm diameter and 0.8 μm pore size (PC; Adavantec, Japan). After drying for 3 hours at 60℃, CNTs and GP were fixed on the membranes. Scaffolds were sterilized by ultraviolet radiation for 24 hours prior to experiments with cells. The morphology of scaffolds was examined by scanning electron microscopy (SEM; S–4000, Hitachi, Japan).

Evaluation of protein adsorption on scaffolds

For the evaluation of protein adsorption on scaffolds, each scaffold was immersed in 2 mL of Dulbecco's modified Eagle's medium (DMEM; SIGMA) with 10% fetal bovine serum (FBS; Biowest) used for cell culture. After 24 hours incubation at 37℃, the substrates were washed three times with PBS, sonicated for 15 minutes, and centrifuged (12000 rpm) for 3 minutes to separate proteins from the substrates. Aliquots of the removed solution were analyzed by the BCA method.

Cell culture

The scaffolds were placed in polystyrene dishes of 60 mm diameter. Then, 1.0×10^5 human osteoblast-like cells (SaOS2) were seeded onto each scaffold and cultured in Dulbecco's modified Eagle's medium (DMEM; SIGMA) with 10% fetal bovine serum (FBS; Biowest) and 1% penicillin-streptomycin under the standard cell culture conditions (at 37℃ in a humidified 5% CO_2/95% air environment) for 3 and 7 days. The medium was changed every other day.

Cell proliferation

For the evaluation of cell proliferation, cells were cultured for 3 and 7 days on the substrates. Cell proliferation was evaluated by counting the number of cells attached to each scaffold in SEM micrographs. For SEM observation, at the end of each prescribed time period, the substrates were rinsed with PBS to remove non-adherent cells on the membranes, fixed in a solution of 2% glutaraldehyde, and post-fixed in a 1% osmium tetroxide solution. The samples were then dehydrated in a series of solutions with increasing ethanol concentrations, followed by critical-point drying at 40℃. All the experiments were repeated four times. The numbers of cells were counted in 10 random fields per scaffold and averaged. Objects less than 10 μm in diameter were not included in the attached cell count.

Alkaline phosphatase activity

Alkaline phosphatase (ALP) activity was measured with LabAssay ALP (Wako, Japan). The culture medium was removed and the dishes were rinsed three times with PBS. Cells on the substrates were scraped, incubated with 1000 μl of CelLytic-M (Sigma) for 15 minutes on a shaker, and centrifuged (500 g) for 15 minutes. Samples of 20 μl were added to 100 μl of *p*-nitrophenol phosphatase in a carbonate buffer and incubated for 15 minutes at 37℃. After 80 μl of NaOH was added, absorbance was measured at 405 nm (Benchmark, Bio-Rad, USA) and enzyme activity was determined from the calibration curve of *p*-nitrophenol standard. ALP activity was normalized by total protein content measured by a BCA protein assay kit (Pierce, USA) and expressed as μmol *p*-nitrophenol/mg protein.

Statistical analysis

All the experiments on protein adsorption, cell proliferation, and ALP activity were repeated four times. Statistical significance between groups was calculated using the Mann-Whitney U test with Bonferroni correction under the condition of $p<0.05$.

RESULTS

SEM images of scaffolds

Fig. 1 shows the SEM images of scaffolds. GP (b) on PC (a) was a particle of about 5 μm in size. There were little differences in the fibrous morphology between MW (c) and SW (d) on PC. Both CNTs formed a densely packed meshwork nanostructure (Figs. 1(c) and (d)). The diameter of SW resembled that of MW, coupled with a formation of bundles.

Cell morphology

Fig. 2 shows the SEM images of the morphology of SaOS2 cells cultured for 3 and 7 days on each

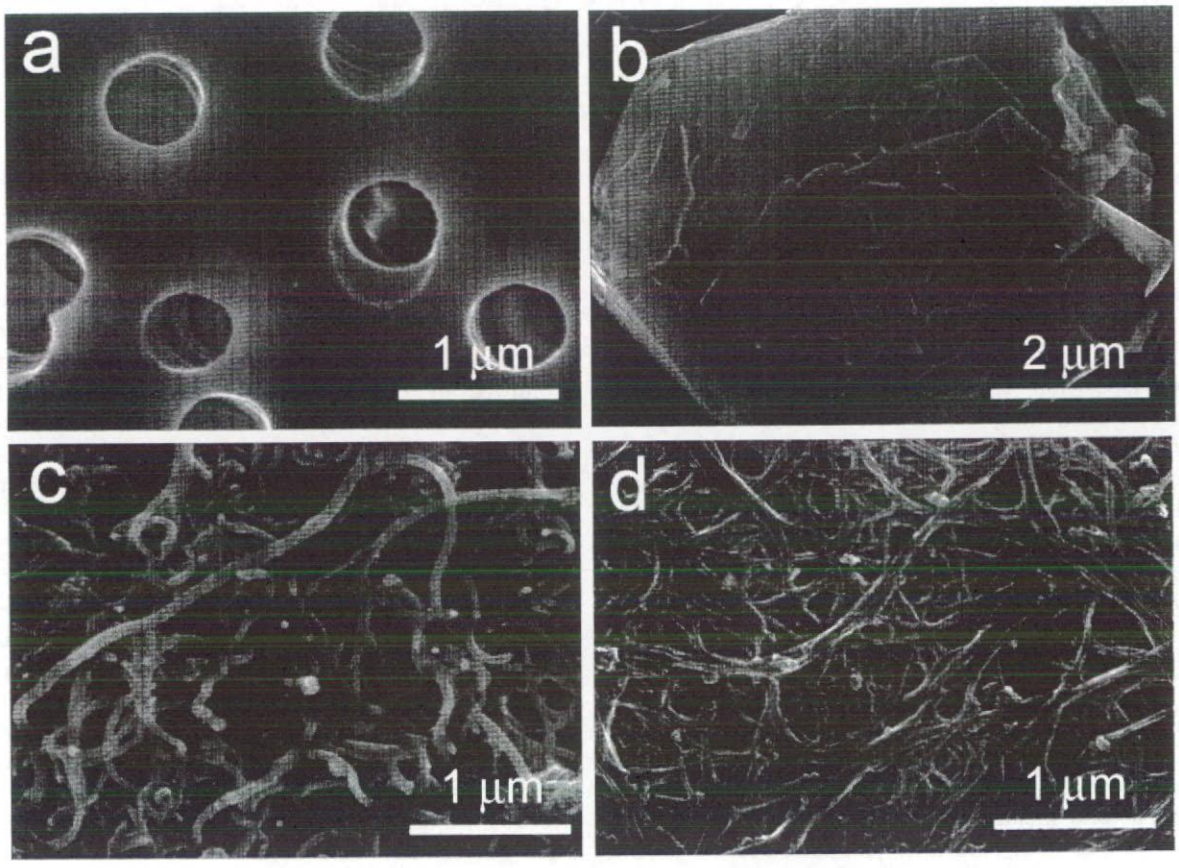

Fig. 1 SEM images of scaffolds: PC (a), GP (b), MW (c), and SW (d).

scaffold. Except on GP, cells proliferated and spread with incubation time. The cells on SW grew nearly to confluence after 7 days. The morphology of the cells on CNTs was markedly different from that on non-CNT scaffolds. Most of the cells on PC were elongated in one direction (Fig. 2(a)) and those on GP were round (Fig. 2(b)), whereas those on CNTs extended in all directions and proliferated well (Figs. 2(c) and (d)). As for comparison between MW and SW, it could be seen that the cells exhibited similar morphology.

Amount of adsorbed proteins on scaffolds

Fig. 3 shows the amounts of adsorbed proteins on the scaffolds immersed in cell culture medium after 24 hours. Proteins in medium were adsorbed to a certain extent depending on the substrate. CNT scaffolds showed higher values than PC and GP. Between CNTs, adsorption on SW was about twice as high as that on MW.

Cell proliferation

Fig. 4 shows the number of proliferated SaOS2 cells after 3 and 7 days. Few cells were attached and proliferated on GP. The number of cells attached to the CNTs was significantly larger than on PC and GP for all the proliferation periods ($p<0.05$). Between CNTs, the number of cells on SW was similar to that on MW at 3 days, but significantly increased to 2.7 times that of MW at 7 days ($p<0.05$).

Alkaline phosphatase activity

Fig. 5 shows the ALP activity (expressed as *p*-nitrophenol mmol/L) of the cells on each substrate at 3 and 7 days. The ALP activity increased with time for all the substrates. CNTs showed higher activity than PC and GP and increased from 3 to 7 days. SW showed the highest increase of ALP activity at 7 days.

Fig. 6 shows the ALP activity normalized by total protein content at 3 and 7 days. Except for GP, the ALP activity increased with time for all the substrates. Nonetheless, CNTs showed higher activity than PC at 3 and 7 days. For scaffolds made of carbon, they were similar at 3 days but SW was the highest at 7 days.

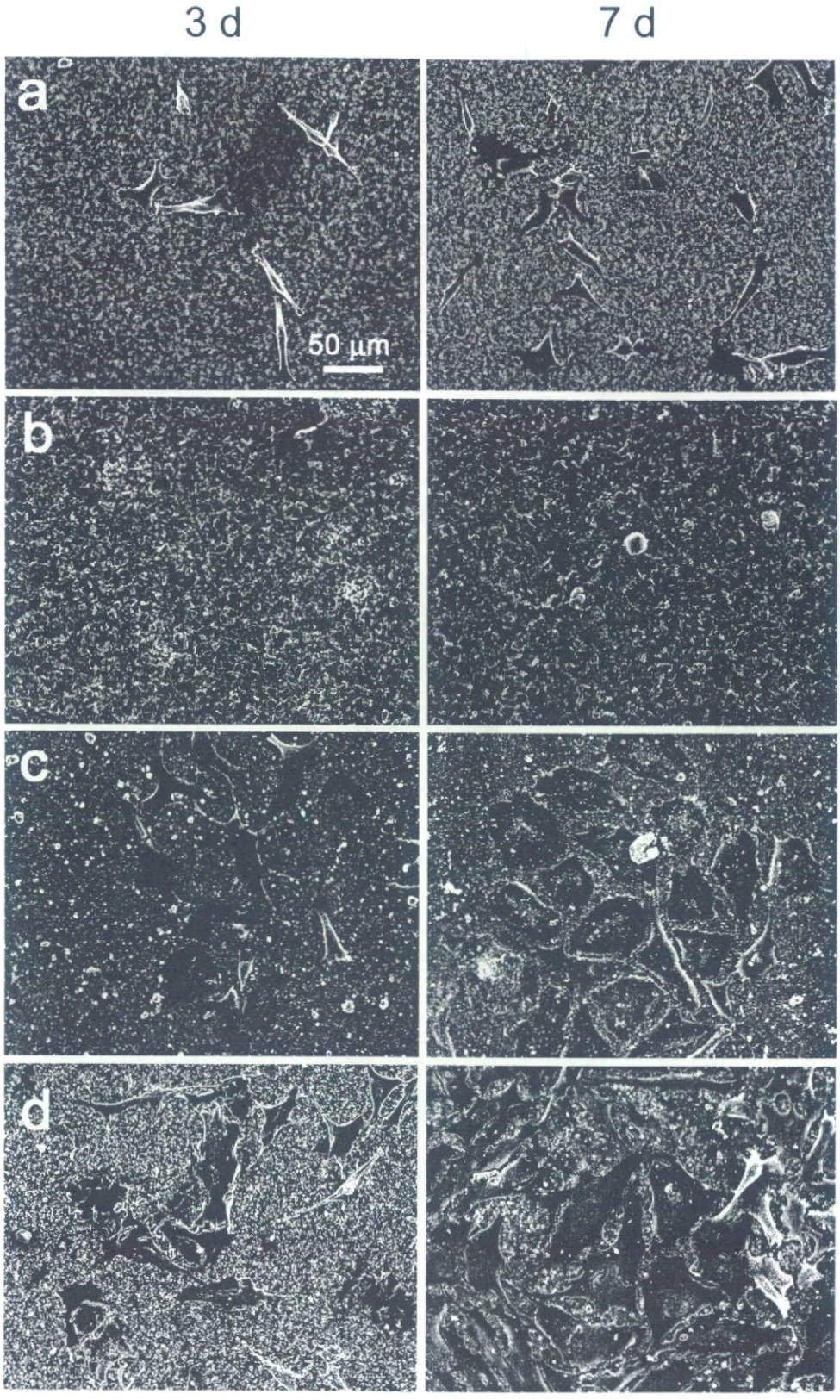

Fig. 2 SEM images of cells cultured for 3 days (left) and 7 days (right) on: PC (a), GP (b), MW (c), and SW (d).

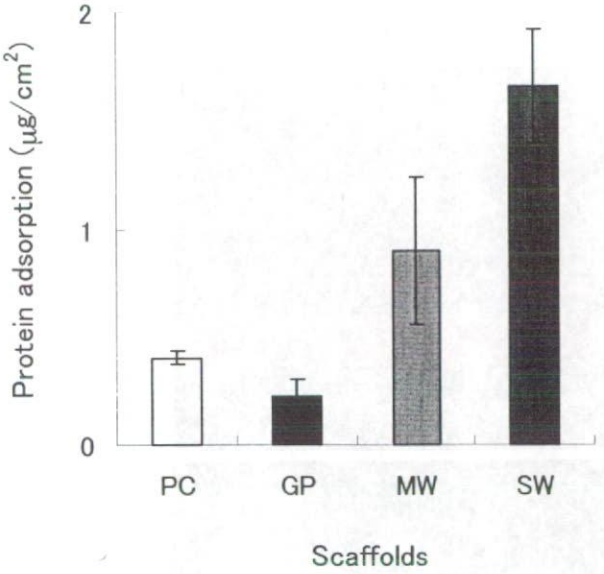

Fig. 3 Amounts of adsorbed proteins on the scaffolds immersed in cell culture medium after 24 h.

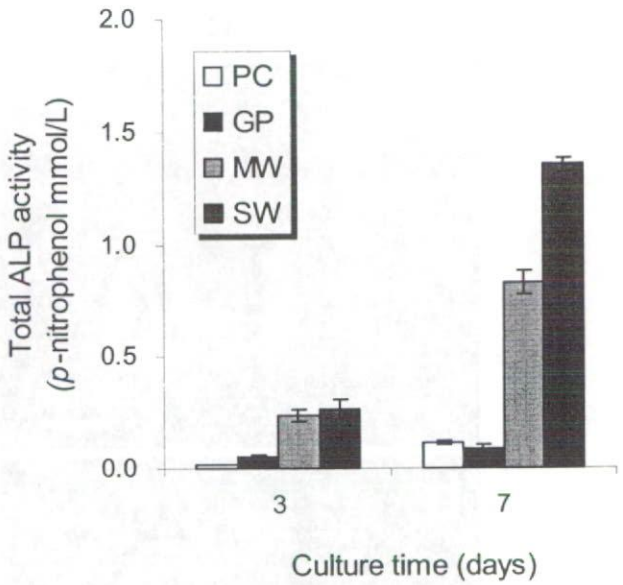

Fig. 5 Total ALP activity of cells cultured on the scaffolds at 3 and 7 days.

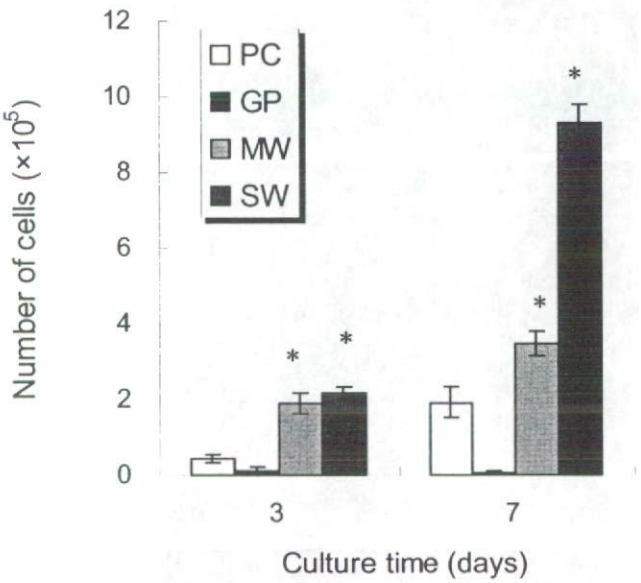

Fig. 4 Number of SaOS2 cells cultured on the scaffolds at 3 and 7 days, where '*' indicates significant difference at $p<0.05$ upon comparison between respective substrates at 3 and 7 days.

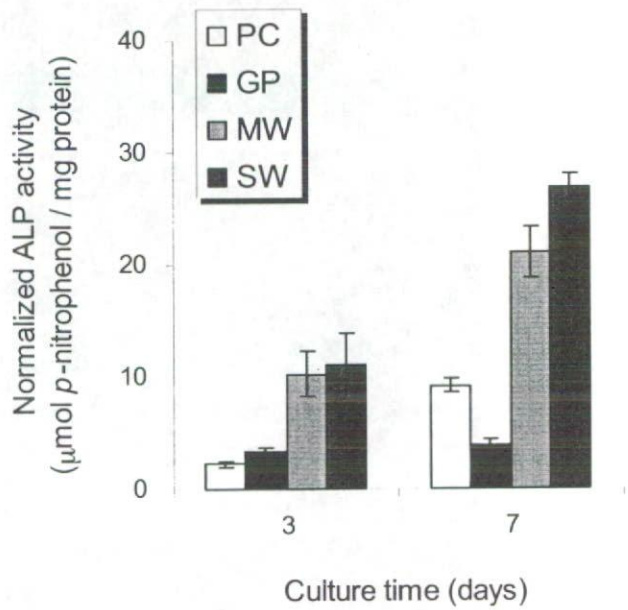

Fig. 6 ALP activity normalized by total protein content in a μmol p-nitrophenol/mg protein unit.

DISCUSSION

Cell morphology

The present *in vitro* study demonstrated that cell morphology was affected by the scaffolds. SEM images showed that CNT scaffolds presented a fibrous nanostructure, while PC and GP scaffolds had microporous or microparticle structure, respectively. Scaffolds should have properties favorable for cell attachment and growth[21]. Cells that develop in a flat form with a small contact angle have stronger binding and affinity to the scaffold than those that are round with a large contact angle[17]. The present study showed that the cells on CNTs extended in all directions, whereas cells on PC and GP had a spindle or round shape. Our previous studies showed that cells on MW extended in all directions[16,17]. Similarly, cells on SW showed strikingly extended morphology with a diameter of approximately 100 μm. The morphology of osteoblasts that spread flatly on CNTs resembled the case of titanium which has good biocompatibility[28]. Thus, it could be said that CNTs

showed favorable properties for cell growth.

Cell proliferation

The number of cells that proliferated on CNTs was larger than on PC and GP. SW in particular showed near confluence at 7 days and the largest proliferation rate from 3 to 7 days. Cell proliferation is influenced by surface characteristics such as topography[29] and the chemical state[30,31]. A nanoporous structure was found to provide a favorable surface architecture for osteoblast function[32]. In this study, the large number of attached cells on CNT scaffolds could be attributed to the nanostructures with high porosity and a specific surface area.

Protein adsorption on scaffolds

CNTs have the ability to adsorb various molecules non-specifically[33,34]. As it is very likely that adsorbed proteins in serum influence the properties for cell proliferation and growth, protein adsorption on the scaffolds was evaluated in this study. Adsorption of proteins was higher on SW than on other substrates. Therefore, in addition to surface topography, this might further enhance cell proliferation and growth. For GP, its nonthrombogenic property made it difficult for various molecules to be adsorbed on the surface, and thus it is used for heart valve prosthetics[35]. As a result, although both CNTs and GP consisted of carbon, their cell responses were quite different. On CNTs with the surface modified by various proteins and other molecules, cell proliferation and growth were easier. This was a chief reason why cell proliferation and growth were excellent on SW.

Cell functions

The functional activity of proliferated cells and its dependence on scaffolds were evaluated by measuring the ALP activity, which is the most commonly used markers for bone formation of osteoblast cells[36]. Total ALP was the whole amount synthesized by the cells proliferated on the scaffolds. Normalized ALP activity was expressed as activity per unit protein, which could compare qualitatively the degree of activity for each scaffold system. According to the normalized ALP activity (Fig. 6), cells on GP were inert with respect to bone formation, while those on CNTs had high activity. Further, cell proliferation on SW was higher than on MW (Fig. 4). From the results on the number of cells cultured (Fig. 4) and total ALP activity (Fig. 5), cell function per cell on MW was higher than that on SW. These results thus further indicated that proliferation and ALP activity were expected to follow trends of lower proliferation and increased ALP production for porous scaffold[37].

Origin of biocompatibility of CNTs

The present study investigated the cellular response of osteoblasts to various carbon materials: GP, MW, and SW. On CNTs there was efficient cell proliferation and function, whereas there was very little on GP. Cellular response depends on the chemical properties of the substrate, and CNT surface can be modified with various molecules. In the present case, proteins in culture medium were adsorbed on CNTs but very minimally so on GP, as seen in Fig. 3. Our previous study also showed that apatite was precipitated on CNTs when they were immersed in a simulated body fluid[33]. Taken together, the different surface chemical properties between CNTs and GP might originate or stem from their different crystal structures. As a result, although both CNTs and GP were composed of graphene sheets, they demonstrate different affinities toward proteins.

In addition, CNT scaffolds had a high specific surface area due to the small diameter of the CNTs and the porosity of the network structure. As a result, culture medium was easily soaked into the dense meshwork nanostructure formed by the CNTs. In other words, uptake of nutrition and molecules necessary for the extracellular matrix for cell adhesion and growth could be easily done through the mesh-like structure. These factors then led to the high cell adhesion, proliferation, spreading, and growth of filopodia on CNTs.

Carbon as a raw material is originally bioinert in terms of its chemical properties. The topological features of the nanonetwork assembly and the surface modification by apatite precipitation and protein adsorption served to convert CNTs into a bioactive material with pronounced cell proliferation and functional activities.

CONCLUSIONS

Although GP, MW, and SW were isomorphs composed only of carbon atoms, their osteoblast cell responses in terms of cell morphology, cell proliferation, and ALP activity were quite different. With CNTs, cell growth, proliferation, and functions were higher than GP. In particular, cell proliferation and total ALP activity on SW were higher than on MW. These results could be due to the surface topology and chemical properties of the substrates. The former was the dense meshwork nanostructure of CNTs. The latter was the protein adsorption on CNT surface in the cell culture medium. Together, these properties made the CNTs well poised as scaffold materials for cell culture.

ACKNOWLEDGEMENTS

This research was supported in part by Health and

Labor Sciences Research Grants for Research on Chemical Substance Assessment from the Ministry of Health, Labor and Welfare, Japan (H18-Chemistry-General-006), and by Grants (Nos. 16390549 and 17659602) from the Ministry of Education, Sports, Science and Technology, Japan.

REFERENCES

1) Feynman R. There's plenty of room at the bottom. Science 1991; 254:1300-1301.
2) Siegel RW. Creating nanophase materials. Sci Am 1996; 275:42-47.
3) Labhasetwar V. What is next for nanotechnology? J Biomed Nanotechnol 2005; 1:373-374.
4) Park GE, Webster TJ. A review of nanotechnology for the development of better orthopedic implants. J Biomed Nanotechnol 2005; 1:18-29.
5) Iijima S. Helical microtubules of graphitic carbon. Nature 1991; 354:56-58.
6) Uo M, Tamura K, Sato Y, Yokoyama A, Watari F, Totsuka Y, Tohji K. The cytotoxicity of metal-encapsulating carbon nanocapsules. Small 2005; 1:816-819.
7) Harrison BS, Atala A. Carbon nanotube applications for tissue engineering. Biomaterials 2007; 28:344-353.
8) Chlopek J, Czajkowska B, Szaraniec B, Frackowiak E, Szostak K, Béguin F. *In vitro* studies of carbon nanotubes biocompatibility. Carbon 2006; 44:1106-1111.
9) Lovat V, Pantarotto D, Lagostena L, Cacciari B, Grandolfo M, Righi M, Spalluto G, Prato M, Ballerini L. Carbon nanotube substrates boost neuronal electrical signaling. Nano Lett 2005; 5:1107-1110.
10) Tian F, Cui D, Schwarz H, Estrada GG, Kobayashi H. Cytotoxicity of single-wall carbon nanotubes on human fibroblasts. Toxicol *In Vitro* 2006; 20:1202-1212.
11) Bottini M, Bruckner S, Nika K, Bottini N, Bellucci S, Magrini A, Bergamaschi A, Mustelin T. Multi-walled carbon nanotubes induce T lymphocyte apoptosis. Toxicol Lett 2006; 160:121-126.
12) Monteiro-Riviere NA, Nemanich RJ, Inman AO, Wang YY, Riviere JE. Multi-walled carbon nanotube interactions with human epidermal keratinocytes. Toxicol Lett 2005; 155:377-384.
13) Cui D, Tian F, Ozkan CS, Wang M, Gao H. Effect of single wall carbon nanotubes on human HEK293 cells. Toxicol Lett 2005; 155:73-85.
14) Yokoyama A, Sato Y, Nodasaka Y, Yamamoto S, Kawasaki T, Shindoh M, Kohgo T, Akasaka T, Uo M, Watari F, Tohji K. Biological behavior of hat-stacked carbon nanofibers in the subcutaneous tissue in rats. Nano Lett 2005; 5:157-161.
15) Wang W, Omori M, Watari F, Yokoyama A. Novel bulk carbon nanotube materials for implant by spark plasma sintering. Dent Mater J 2005; 24:478-486.
16) Aoki N, Yokoyama A, Nodasaka Y, Akasaka T, Uo M, Sato Y, Tohji K, Watari F. Cell culture on a carbon nanotube scaffold. J Biomed Nanotechnol 2005; 1:402-405.
17) Aoki N, Yokoyama A, Nodasaka Y, Akasaka T, Uo M, Sato Y, Tohji K, Watari F. Strikingly extended morphology of cells grown on carbon nanotubes. Chem Lett 2006; 35:508-509.
18) Langer R, Vacanti JP. Tissue engineering. Science 1993; 260:920-926.
19) Desai TA. Micro- and nanoscale structures for tissue engineering constructs. Med Eng Phy 2000; 22:595-606.
20) Zanello LP, Zhao B, Hu H, Haddon RC. Bone cell proliferation on carbon nanotubes. Nano Lett 2006; 6:562-568.
21) Olivier V, Faucheux N, Hardouin P. Biomaterial challenges and approaches to stem cell use in bone reconstructive surgery. DDT 2004; 9:803-811.
22) Sachlos E, Czernuszka JT. Making tissue engineering scaffolds work. Eur Cells Mater 2003; 5:29-39.
23) Correa-Duarte MA, Wagner N, Rojas-Chapana J, Morsczeck C, Thie M, Giersig M. Fabrication and biocompatibility of carbon nanotube-based 3D networks as scaffolds for cell seeding and growth. Nano Lett 2004; 4:2233-2236.
24) Mattson MP, Haddon RC, Rao AM. Molecular functionalization of carbon nanotubes and use as substrates for neuronal growth. J Mol Neurosci 2000; 14:175-182.
25) Webster TJ, Waid MC, McKenzie JL, Price RL, Ejiofor JU. Nano-biotechnology: carbon nanofibers as improved neural and orthopedic implants. Nanotechnology 2004; 15:48-54.
26) MacDonald RA, Laurenzi BF, Viswanathan G, Ajayan PM, Stegemann JP. Collagen-carbon nanotube composite materials as scaffolds in tissue engineering. J Biomed Mater Res A 2005; 74:489-496.
27) Sato Y, Yokoyama A, Shibata K, Akimoto Y, Ogino S, Nodasaka Y, Kohgo T, Tamura K, Akasaka T, Uo M, Motomiya K, Jeyadevan B, Ishiguro M, Hatakeyama R, Watari F, Tohji K. Influence of length on cytotoxicity of multi-walled carbon nanotubes against human acute monocytic leukemia cell line THP-1 *in vitro* and subcutaneous tissue of rats *in vivo*. Mol Biosyst 2005; 1:176-182.
28) Watari F, Yokoyama A, Omori M, Hirai T, Kondo H, Uo M, Kawasaki T. Biocompatibility of materials and development to functionally graded implant for bio-medical application. Compos Sci Technol 2004; 64:893-908.
29) Yuda A, Ban S, Izumi Y. Biocompatibility of apatite-coated titanium mesh prepared by hydrothermal-electrochemical method. Dent Mater J 2005; 24:588-595.
30) Anselme K. Osteoblast adhesion on biomaterials. Biomaterials 2000; 21:667-681.
31) Deligianni DD, Katsala ND, Koutsoukos PG, Missirlis YF. Effect of surface roughness of hydroxyapatite on human bone marrow cell adhesion, proliferation, differentiation and detachment strength. Biomaterials 2000; 22:87-96.
32) Popat KC, Leary Swan EE, Mukhatyar V, Chatvanichkul KI, Mor GK, Grimes CA, Desai TA. Influence of nanoporous alumina membranes on long-term osteoblast response. Biomaterials 2005; 26:4516-4522.
33) Akasaka T, Watari F. Nano-architecture on carbon nanotube surface by biomimetic coating. Chem Lett 2005; 34:826-827.
34) Bianco A, Kostarelos K, Prato M. Applications of carbon nanotubes in drug delivery. Curr Opin Chem Biol 2005; 9:674-679.
35) Milligan HL, Davis JW, Edmark KW. The search for

the nonthrombogenic property of colloidal graphite. J Biomed Mater Res 1970; 4:121-138.
36) Delmas PD. Clinical use of biochemical markers of bone remodeling in osteoporosis. Bone 1992; 13:S17-S21.
37) St-Pierre JP, Gauthier M, Lefebvre LP, Tabrizian M. Three-dimensional growth of differentiating MC3T3-E1 pre-osteoblasts on porous titanium scaffolds. Biomaterials 2005; 26:7319-7328.

Mechanical Properties and Biological Behavior of Carbon Nanotube/Polycarbosilane Composites for Implant Materials

Wei Wang,[1] Fumio Watari,[1] Mamoru Omori,[2] Susan Liao,[1] Yuhe Zhu,[1] Atsuro Yokoyama,[1] Motohiro Uo,[1] Hisamichi Kimura,[2] Akira Ohkubo[2]

[1] Graduate School of Dental Medicine, Hokkaido University, Sapporo 060-8586, Japan

[2] Advanced Research Center of Metallic Glasses, Institute for Materials Research, Tohoku University, Sendai 980-8577, Japan

Received 20 January 2006; revised 29 June 2006; accepted 22 August 2006
Published online 20 December 2006 in Wiley InterScience (www.interscience.wiley.com). DOI: 10.1002/jbm.b.30724

Abstract: Multiwalled carbon nanotube/polycarbosilane (MWCNT/PCS) composites were fabricated by the spark plasma sintering (SPS) method. The MWCNT/PCS composites consisted of MWCNTs and nanosized SiC particles pyrolyzed from PCS and possessing good mechanical properties for bone tissue repair or dental implantation. The MWCNT/PCS composites were implanted in the subcutaneous tissue and femur of rats at 1 and 4 weeks after implantation. Histological investigations showed that there was little inflammatory response in the subcutaneous tissue, and newly formed bone tissue was observed in the femur. These results indicated that the MWCNT/PCS composite had little prophlogistic effect and good osteoconductivity. The study suggested the possibility that the MWCNT/PCS composite could be a candidate bone-substitute and dental-implant material in the future. © 2006 Wiley Periodicals, Inc. J Biomed Mater Res Part B: Appl Biomater 82B: 223–230, 2007

Keywords: carbon nanotube/polycarbosilane; spark plasma sintering; mechanical properties; biocompatibility; implant

INTRODUCTION

Conventional carbon materials such as carbon fibers with dimensions in the micron range possessing exceptionally high mechanical properties have also long been considered as biomaterials, e.g., as substitutes for soft tissue of cartilage, tendons, and blood vessels using collagen/carbon fiber composites.[1–7] However, a clinical study observed severe foreign-body reactions around carbon fibers implanted into the right knees of patients after 6 months, which indicated that conventional carbon materials might not be optimal biomaterials.[8]

Multiwalled carbon nanotubes (MWCNTs), are similar to hollow graphite fibers, except that they have a much higher degree of structural perfection.[9–11] They have attracted a great deal of attention in the large international community interested in the fundamental nanoscience of these molecular filaments as well as the possibilities for new technology. Their graphite-like-structure tube wall and the nanometer-sized channel, make them promising in such applications as storage of hydrogen, as some polymer additives, and as catalyst support materials. Recently, some scientists have considered the use of carbon nanotubes as biomaterials and some studies indicated that they showed better bioactivity than conventional carbon materials.[12–15] MWCNTs possess excellent mechanical, electrical, and surface properties compared to conventional carbon fibers.[16–18] They also have a density even smaller than graphite and high porosity due to the tubular structure. Thus, if they can be consolidated as a bulk material with sufficient high strength, bulk MWCNT materials may be used for implants with light weight or for functional biomaterials such as new drug delivery systems (DDS) in the medical field. However, no study on bulk CNT materials with sufficient strength to be used as implant materials has been reported yet due to the general difficulty of fabricating bulk CNTs. Recently the spark plasma sintering (SPS) method has been developed, and various ceramics, composites, and other materials that are difficult to sinter, including hydroxyapatite (HAP), Ti, and functionally graded materials (FGM), have been successfully consolidated.[19–24] By efficiently charging electrical energy and applying highly energized electrical spark discharges momentarily to powder particles, bulk CNTs could be fabricated at relatively low temperature and pressure with a short holding time, which would be advantageous to restrain excessive grain growth.[25–27] In the present study, we successfully prepared bulk MWCNTs using polycarbosilane (PCS), a silicon carbide precursor, as

Correspondence to: W. Wang (e-mail: ww1120@den.hokudai.ac.jp)
Contract grant sponsors: Ministry of Health, Labour and Welfare, Japan and Advanced Research Center of Metallic Glasses, Institute for Materials Research, Tohoku University

a binder by adopting the SPS method. The PCS and SPS sintering conditions were optimized to increase strength, and the mechanical properties and biocompatibility of bulk MWCNT/PCS composites were investigated.

MATERIALS AND METHODS

Preparation of Composite

MWCNTs (Nano Lab Co.) of (20–40) nm φ × (5–20) μm with purity 80% were refined. MWCNTs were baked at 500°C for 90 min, and then immersed in and rinsed with 6*M* hydrochloric acid solution several times to dissolve the metallic catalysts attached at their extremities, followed by filtering with a membrane filter, washing with deionized water and drying for 24 h at 60°C. Finally, purified products were obtained.

The 20, 30, 40 wt % PCS (Sumitomo Osaka Cement) were dissolved in hexane, and the refined MWCNT powders mixed with the solution. After the evaporation of hexane, the mixed powders were packed into a $\varphi = 20 \times 10$ mm^2 mold, then sintered by SPS (Ultra-High Temperature Synthesis-Spark Plasma System Dr Sinter 1050, Sumitomo Coal Mining Co., Tokyo, Japan). SPS treatment was carried out in three steps: first, at 600°C for 18 min with the pressure maintained constant at 60 MPa, next at 800°C for 5 min with 120 MPa pressure, then at 1000°C for 15 min under 40 MPa pressure. Finally, specimens were cooled to room temperature in the SPS chamber. The sintered cylinder block was cut into rectangular rods for mechanical and animal implantation tests using a diamond disk.

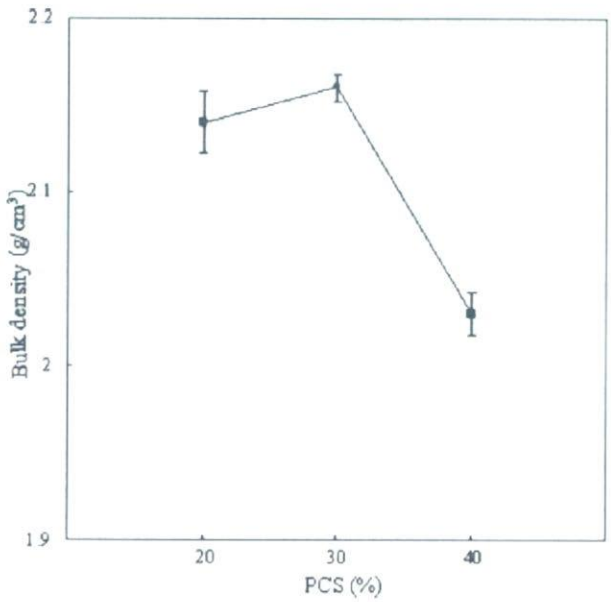

Figure 1. Dependence of bulk density of the sintered MWCNTs on PCS content.

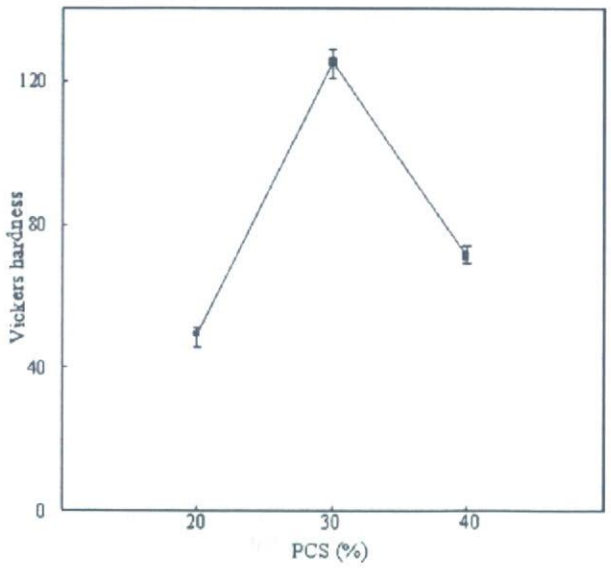

Figure 2. Dependence of Vickers hardness of the sintered MWCNTs on PCS content.

Mechanical Test, Observation, and Analysis

Bulk density was measured with deionized water as the immersion medium according to Archimedes' principle. Micro Vickers hardness was measured using a tester (NT-M001, Daojing Company). The three point flexural test was done for the bar specimens ($2 \times 2 \times 10$ mm^3) using a universal testing machine (Instron, Model 4204), and the elastic modulus was calculated. A compressive test was done for the bar specimens ($3 \times 3 \times 5$ mm^3) using the universal testing machine. Observation of the MWCNT/PCS material

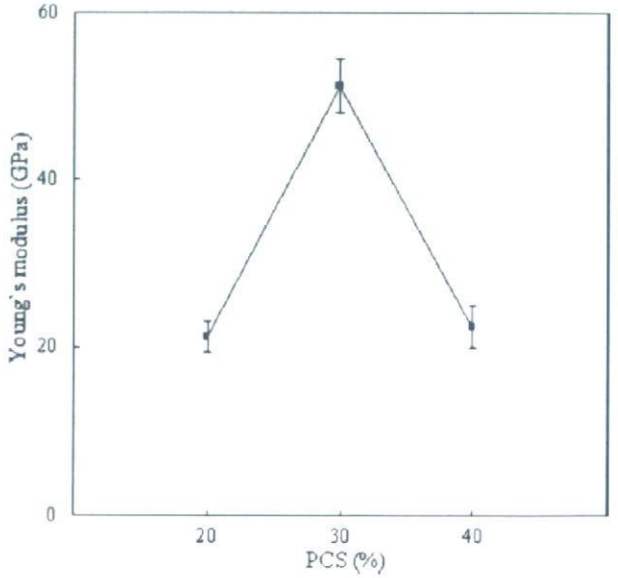

Figure 3. Dependence of Young's modulus of the sintered MWCNTs on PCS content.

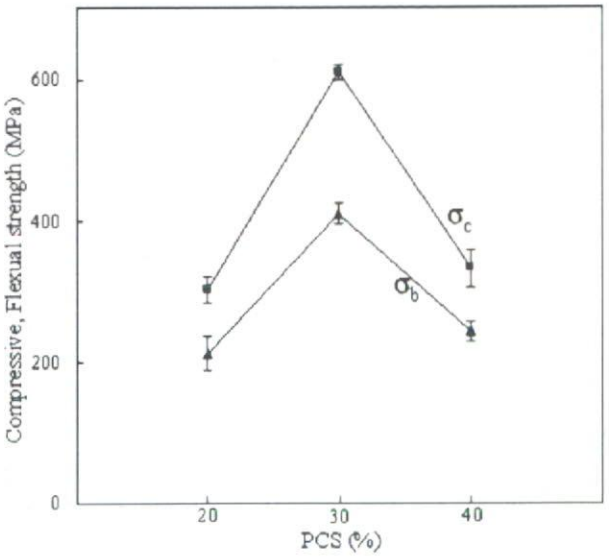

Figure 4. Compressive strength σ_c and flexural strength σ_b of the sintered MWCNTs.

was carried out by transmission electron microscopy (TEM/Hitachi, H-800, Japan) and scanning electron microscopy (SEM/Hitachi, S-4000, Japan). Identification of crystal phases was done using an X-ray diffractometer (XRD/Multiflex, Rigaku Corporation, Japan).

Histological Evaluation

The MWCNT/20% PCS and MWCNT/30% PCS composites were cut into a rod shape ($1 \times 1 \times 5$ mm^3), washed in ethanol by ultrasonication, and sterilized with an autoclave. They were employed for the animal experiment using eight Wister-strain rats aged 12 weeks (weight 400–420 g). After the rats were anesthetized with diethyl ether (Wako Pure Chemical Industries, Osaka, Japan), pentobarbital sodium (6 mg/kg; Nembutal Injection, Dainabot, Osaka, Japan) was injected into the abdominal. Implantation in the subcutaneous tissue was done into a pocket made in the thoracic region. For hard tissue, a hole was carefully made in the diaphysis of the femur using a dental round bur ($\varphi = 2$ mm), with a physiological saline external coolant, and the materials were inserted into bone marrow. Animal experiments were performed in accordance with the Guide for the Care and Use of Laboratory Animals, Graduate School of Dental Medicine Hokkaido University. During the course of the study no rats were lost.

The rats were sacrificed at 1 and 4 weeks after implantation, and the tissue blocks containing specimens were resected and fixed. The specimens in the subcutaneous tissue were stained with hematoxylin and eosin, and embedded in paraffin. The specimens in the femur were stained with Villanueva bone stain, and embedded in PMMA. After the tissue blocks were sectioned at 400 μm with a precision sawing machine (Isomt 2000, Buehler, IL), the thinner sections of about 100 μm in thickness were prepared by mechanical polishing.

RESULTS

Physical and Mechanical Properties

Stable bulk MWCNT/PCS composites in a cylindrical shape with a diameter 20 mm were successfully obtained for 20, 30, and 40% PCS.

Figure 1 shows the dependence of bulk density of MWCNT/PCS composites on PCS content. The bulk den-

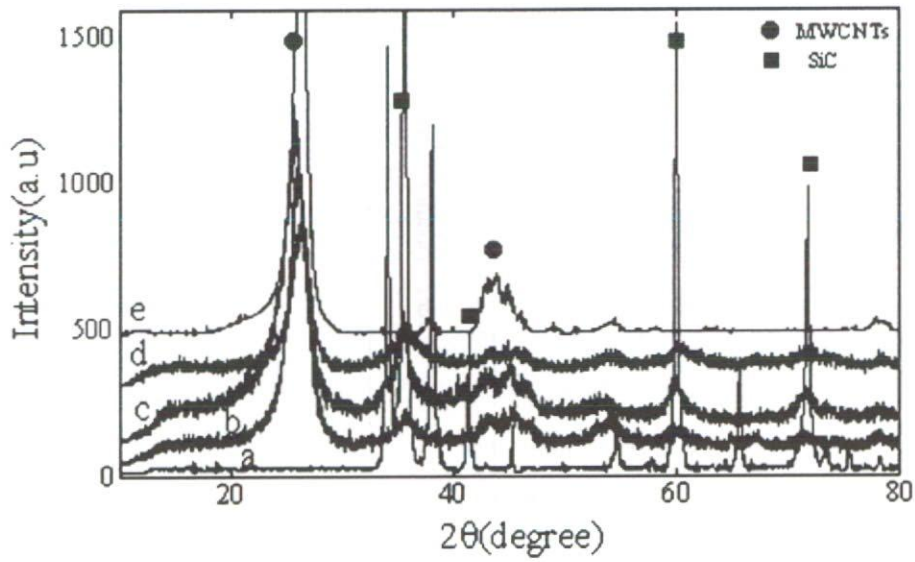

Figure 5. XRD patterns of sintered MWCNTs with 20% PCS (b), 30% PCS (c), and 40% PCS (d), compared with MWCNT powders (e) and SiC powders (a).

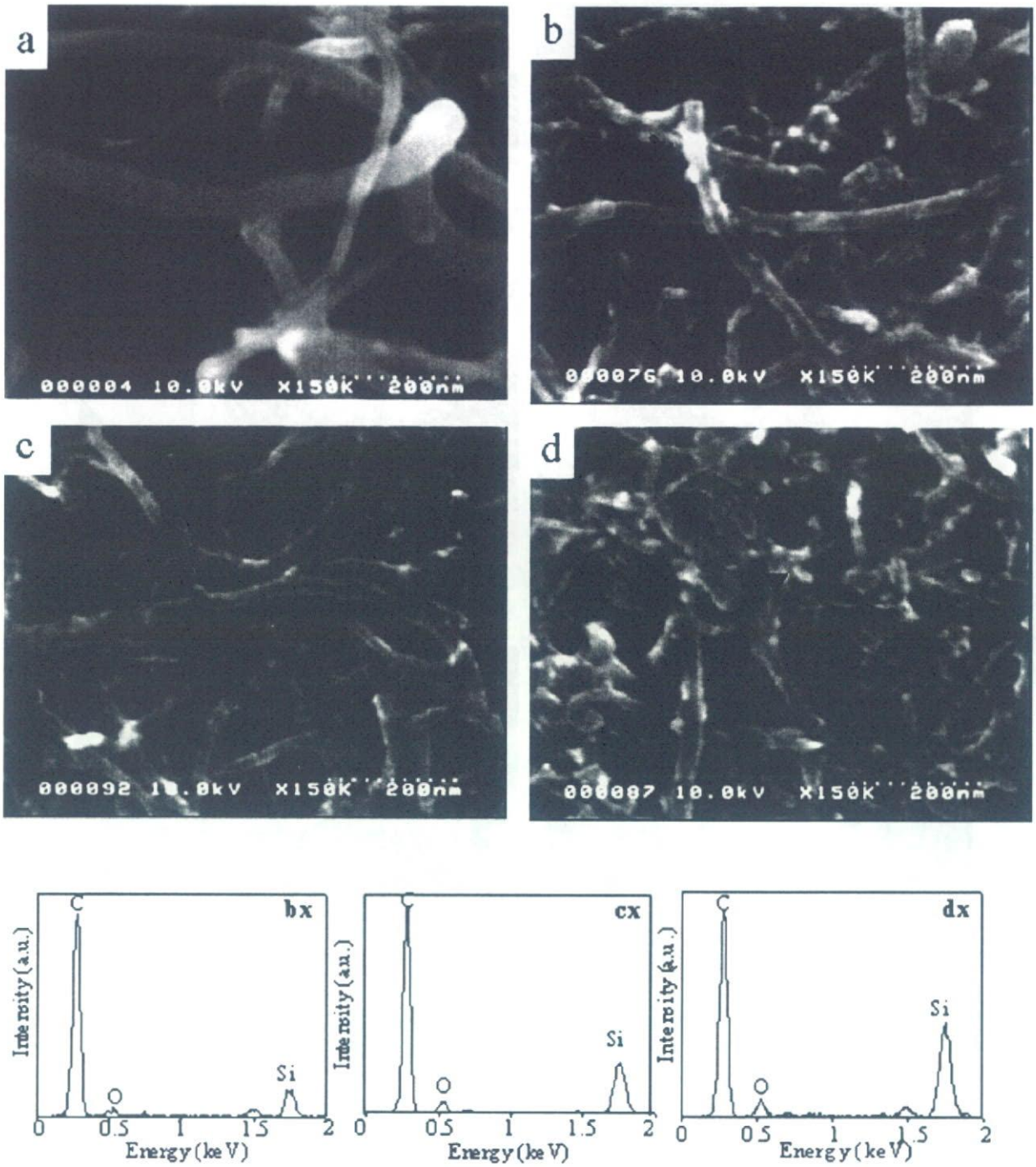

Figure 6. SEM images and corresponding EDS analyses of MWCNTs before sintering (a), MWCNT/20% PCS (b), (bx); MWCNT/30% PCS (c), (cx); and MWCNT/40% PCS (d), (dx).

sity of MWCNT with 30% PCS was slightly higher than that of CNTs with 20% PCS. When PCS content increased to 40%, the bulk density decreased (2.03 g/cm^3). The dependence of the mechanical properties of the MWCNT/PCS material on PCS content is shown in Figure 2 (Vickers hardness), Figure 3 (Young's modulus), and Figure 4 (compressive strength and flexural strength). All these properties showed a similar tendency to exhibit the highest values at 30% PCS and decrease at 40%. The CNTs with 30% PCS had a Vickers hardness of 125, Young's modulus of 51.2 GPa, compressive strength of 608 MPa, and flexural strength of 410 MPa.

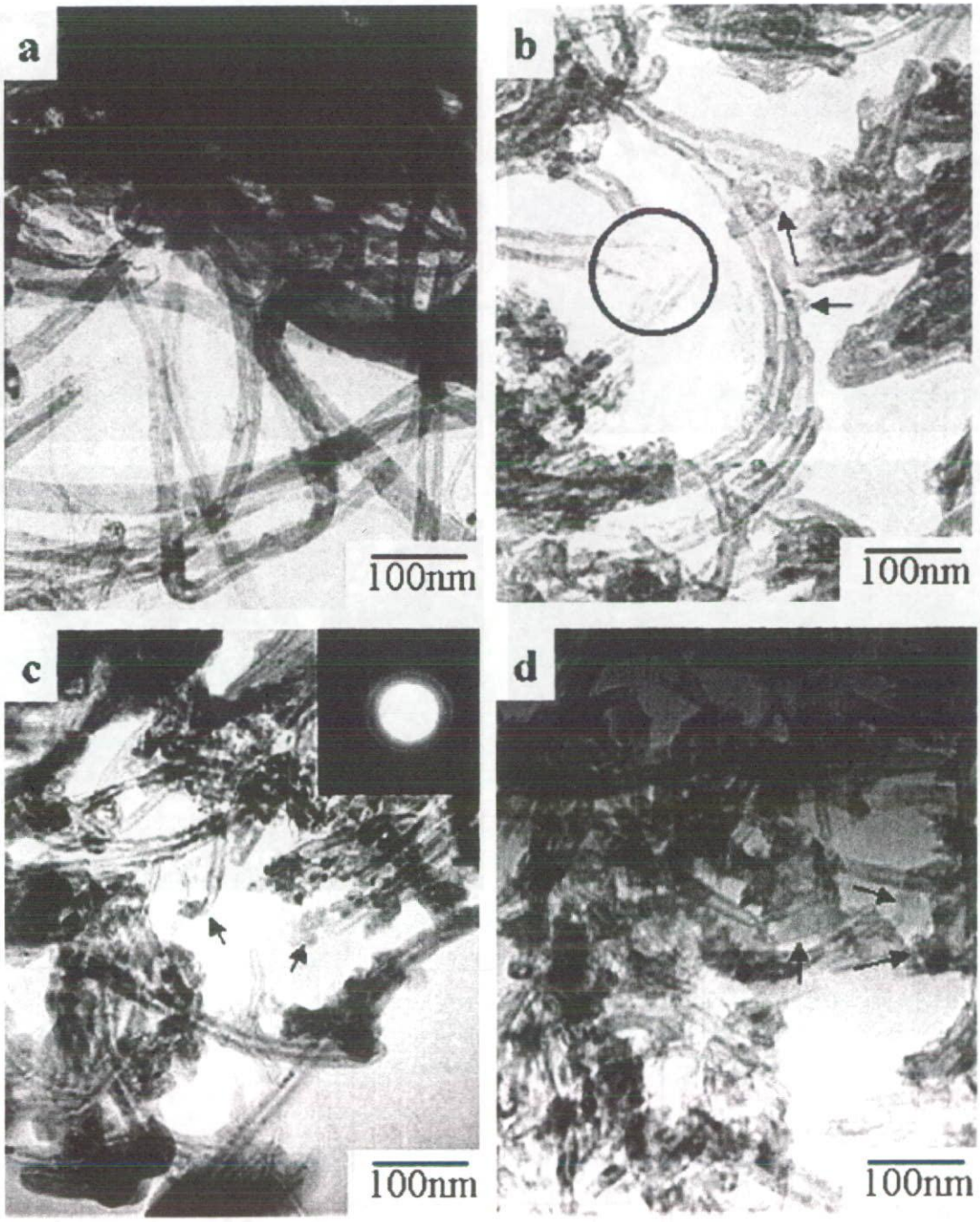

Figure 7. TEM images of MWCNT powders (a), MWCNT/20% PCS (b), MWCNT/30% PCS (c), and MWCNT/40% PCS (d).

XRD Analysis

XRD patterns of MWCNT/PCS composites are shown in Figure 5. The diffraction peaks of both SiC and MWCNTs were observed in all specimens. PCS was pyrolyzed to SiC during the sintering process. The peak width of SiC was broad, suggesting the small size of SiC crystals. For MWCNT/30% PCS, the SiC peaks were sharper than in other specimens.

SEM and TEM Observations

SEM images showed that starting MWCNT powders were entangled with each other and very flexible [Figure 6(a)]. For bulk MWCNTs with 20 and 30% PCS, some nodules adhered on the surfaces of nanotubes, as indicated by arrows in (b,c), and for 40% PCS, more nodules were observed (d). EDX analyses corresponding to the specimens by PCS content are shown in Figures 6 (bx, cx, and

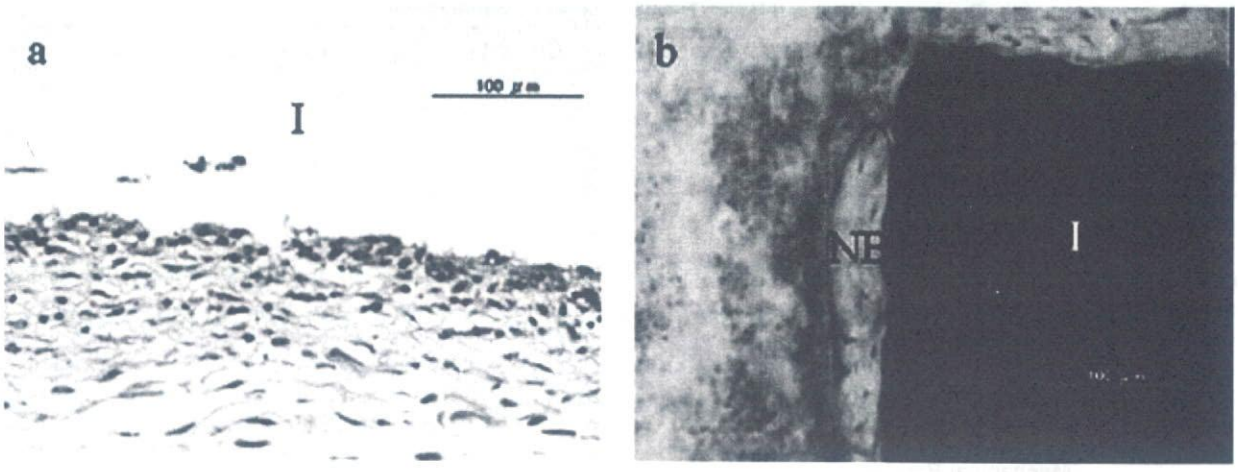

Figure 8. Subcutaneous tissue response (a) and osteogenesis in femur (b) of MWCNTs with 20% PCS at 4 weeks.

dx), and further indicated that bulk MWCNTs consisted of only carbon and silicon, the peak of which was increased with the content of PCS.

No metal catalysts were identified during TEM observation of starting MWCNT powders [Figure 7(a)]. For the bulk MWCNTs with 20, 30, and 40% PCS, a few nanosized nodules were isolated or adhered on the surfaces of nanotubes, as indicated by arrows in Figure 7(b–d). Some of the tips of tubes were open. Such an open-tipped carbon nanotube is shown in the circle of (b). Bulk MWCNT/PCS composites had tubes with external and internal diameters of 40 and 15 nm, respectively, close to the starting CNT powders.

The selected area electron diffraction pattern (SAED) of MWCNT/30% PCS is shown in Figure 7(c), and consisted of five diffraction rings. The first, third, fourth, and fifth rings matched the graphite (002), (100), (004), and (110) reflections. The plane spacing of the second ring, about 0.26 nm, matched the reflection plane of SiC, and probably originated from the nodules adhering on the tube surface.

Histological Evaluation

Subcutaneous Tissue Response. At 1 week after surgery, MWCNT/20% PCS was covered by relatively thick fibrous connective tissue including many cells with large cytoplasm like fibroblasts, fibroblasts with spindle-shaped cytoplasm, and some inflammatory round cells. In addition, dilatation of capillaries was observed around MWCNT/30% PCS. The inflammatory response around MWCNT/30% PCS was greater than that around MWCNT/20% PCS; however, severe inflammation such as necrosis and degeneration was not observed around either. At 4 weeks after implantation, the materials were covered by loose fibrous connective tissue, and inflammation around materials was slight in comparison to that at 1 week [Figure 8(a)]. No difference in the tissue response was observed between MWCNT/20% PCS and MWCNT/30% PCS.

Hard Tissue Response. At 1 week after surgery, active callus formation from the periosteum was observed around both MWCNT/20% PCS and MWCNT/30% PCS. However, new bone did not attach to either material. At 4 weeks, newly formed bone was remodeled to lamellar bone around the materials. Some part of the newly formed bone attached to MWCNT/20% PCS directly [Figure 8(b)], whereas bone marrow and fibrous tissue were observed between bone tissue and MWCNT/30% PCS.

DISCUSSION

Effect of SPS

In this study, to ameliorate the expansion of internal stress and impose the consolidation of MWCNTs, we adopted the SPS sintering method with three steps. The three steps of the sintering method consisted of sintering processes in the following sequence: (1) low temperature/low pressure (600°C, 60 MPa), where an activation effect took place on the powder surface by generating spark plasma, and the plasma could spread between particles; (2) high temperature/high pressure (800°C, 120 MPa), where high temperature and pressure were favorable to consolidate powders; (3) high temperature/low pressure (1000°C, 40 MPa), where low pressure was effective to release the internal stress and the MWCNTs could still further be consolidated under high temperature.

All the results of XRD, SEM, TEM, and SAED indicated that bulk MWCNTs maintained the structure of nanotubes after SPS treatment. This showed that SPS using the three-step sintering method was efficient to create bulk MWCNTs maintaining the tubular structure. With the increase of PCS content, the mechanical properties of MWCNT/PCS materials were the best at 30% PCS, and then decreased at 40% PCS. Addition of too much PCS led to the collapse of the sintered material as a result of the large tensile force

TABLE I. Comparison of the Properties of Sintered MWCNTs with Bone and Other Implants[28]

	Bulk density (g/cm^3)	Vickers hardness	Young's modulus (GPa)	Compressive strength (MPa)	Flexual strength (MPa)
Bone	1.9	<60	19	150	180
Ti	4.15	145	120	550[a]	
HAP	3.15	700	35	600	100
MWCNTs	2.16	125	51.2	608	410

[a] Tensile strength.

imposed by expansion of the mold in the depressurizing process. Addition of 30% PCS was the most suitable and balanced point for the binder to consolidate MWCNTs in the present study. Thus a PCS content of more than 40% was not suitable for the present sintering conditions.

Mechanical Properties

XRD patterns showed that MWCNT/PCS consisted of MWCNTs and SiC pyrolyzed from PCS. For MWCNT/30% PCS, the peak intensity of SiC was sharper than those of MWCNT/20% PCS and MWCNT/40% PCS. This suggested the better crystallinity of SiC crystals at 30% PCS, which was in agreement with the finding that MWCNT/30% PCS possessed the best mechanical properties. The bulk density of the MWCNT/30% PCS material had the highest value, 2.16 g/cm^3, which was much closer to that of human bone 1.6–2.1 g/cm^3, and lower than those of other implant materials: Ti (4.51 g/cm^3) and HAP (3.15 g/cm^3) (Table I).[28] The Young's modulus ranged form 20–50 GPa, with the highest value of 51.2 GPa at MWCNT/30% PCS, higher than that of HAP (35 GPa). The Vickers hardness of MWCNT/30% PCS (125) was slightly smaller than that of Ti (145), and about three times that of bone. The flexural strength of MWCNT/30% PCS was 410 MPa, which was higher than those of HAP (100 MPa) and bone (180 MPa). The bulk MWCNT/PCS materials possessed higher strength than bone but lower than that of Ti, thus satisfying the basic mechanical conditions for hard tissue repair, but remedying the shortcoming of bone resorption around Ti implants with too high strength. The bulk MWCNT/PCS materials possessed a higher Young's modulus and flexural strength than HAP, demonstrating that, compared to HAP, MWCNT/PCS materials have better toughness, which is more suitable for implant materials. The SEM and TEM results showed that the bulk MWCNT/PCS materials maintained the nanotube structure, and SiC pyrolyzed from PCS attached to the tube walls to join the MWCNTs. Such bulk MWCNT/PCS materials with high strength and suitable toughness could be used as new bone substitute materials or implant materials with the ability to slowly release growth factors in the future by using the nanotube structure.

Biocompatibility

Since carbon is a bioinert material, it has long been considered for application in the medical field; however, conventional carbon materials do not necessarily have ideal properties as biomaterials according to the results of clinical studies.[8] Some studies showed that nanophase biomaterials had higher biocompatibility than micron-sized materials.[15,29] Webster et al. reported increased osteoblast adhesion on alumina and titanium with nanometer grain sizes when compared to conventional grain sizes.[30] Moreover, Yokoyama et al. investigated the biological behavior of hat-stacked carbon nanofibers (H-CNFs) in the subcutaneous tissue of rats. The results showed that H-CNFs were englobed by fibrous connective tissue with little inflammation.[14] In a previous study, the biological behavior of nanotubes/nanofibers as a powder or fullerene, but not a structural material, was evaluated.[6,15] In the present study, we investigated the biological response to bulk MWCNT materials with high strength for the first time.

For the response in subcutaneous tissue, there was a difference dependent on the content of PCS in the early implant stage; the degree of inflammation was influenced by SiC pyrolyzed from PCS. The inflammatory response around MWCNT/PCS composites decreased in 4 weeks, and that MWCNT/PCS caused little inflammation. In the response in the femur, after implantation for 4 weeks, the amount of newly formed bone with bulk MWCNTs having 20% PCS was greater than with 30% PCS; however, there was no significant difference in the subcutaneous tissue response between MWCNT/20% PCS and MWCNT/30% PCS. One possible explanation might be that there are many undifferentiated cells and blood vessels in the marrow compared to the subcutaneous tissue and that it is more sensitive to the material properties. Those results showed that the MWCNT/PCS composite had very little prophlogistic effect and possessed osteoconductivity; however, the osteoconductivity was influenced by the PCS content. Therefore, in the future, we are going to study the properties of bulk MWCNTs by changing the PCS content and without PCS.

CONCLUSIONS

The bulk MWCNT/PCS composites were successfully prepared by SPS method with 20, 30, and 40% PCS under the pressure 120 MPa and at a temperature of 1000°C. The bulk MWCNT/PCS composites consisted of MWCNTs maintaining the tubular structure of the starting MWCNT powders and nanosized SiC pyrolyzed from PCS. The bulk MWCNTs with 30% PCS composites added exhibited the best physical and mechanical properties. The tissue

responses and osteogenesis around the implanted materials showed that MWCNT/PCS materials were not prophlogistic. The present study shows that bulk MWCNT/PCS materials have the potential to be applicable as implant materials and for hard tissue repair in the future.

This work was supported by a 2002–2005 Health and Labor Sciences Research Grant for Research on Advanced Medical Technology: "Tissue Reaction and Biomedical Application of Nanotubes, Nanoparticles and Microparticles (H14-Nano-021)", from the Ministry of Health, Labour and Welfare, Japan and the interuniversity cooperative research program of the Advanced Research Center of Metallic Glasses, Institute for Materials Research, Tohoku University.

REFERENCES

1. Price RL, Waid MC, Haberstroh KM, Webster TJ. Selective bone cell adhesion on formulation containing carbon nanofibers. Biomaterials 2003;24:1877–1887.
2. McKenzie JL, Waid MC, Shi R, Webster TJ. Decreased functions of astrocytes on carbon nanofiber materials. Biomaterials 2004;25:1309–1317.
3. Hu H, Ni Y, Montana V, Haddon RC, Parpura V. Chemically functionalized carbon nanotubes as substrates for neuronal growth. Nano Lett 2004;4:507–511.
4. Kus WM, Gorecki A, Strzelczyk P, Swiader P. Carbon fiber scaffolds in the surgical treatment of cartilage lesions. Ann Transplant 1999;4:101,102.
5. Zhang Q, Yang Z, Peng W. Morphological observation of combined-culture of tendon cell or fibroblast of rabbit with artificial materials in vivo. Chin J Reparative Reconstr Surg 1997; 11:103–105.
6. Zhang Q, Yang Z, Peng W. Experiment study in vivo on implantation of autogenous tendon cells after combining culture with carbon fibers. Chin J Reparative Reconstr Surg 1997;11: 168–171.
7. Becker HP, Rosenbaum D, Zeithammel G, Gnann R, Bauer G, Gerngross H, Claes L. Tenodesis versus carbon fiber repair of ankle ligaments: A clinical comparison. Clin Orthop Relat Res 1996;325:194–202.
8. Mortier J, Engelhardt M. Foreign body reaction in carbon filer prosthesis implantation in the keen joint-case report and review of the literature. Z Orthop Ihre Grenzgeb 2000;138: 390–394.
9. Ebbesen TW. Carbon nanotubes: Prepartion and properties. In: Endo M, Saito R, Dresselhaus MS, Dresselhaus G, editors. From Carbon Fibers to Nanotubes. New York: CRC Press; 1997. pp 42–49.
10. Ajiayan PM. Nanotubes from carbon. Chem Rev 1999;99:1787–1799.
11. Dejong KP, Geus JW. Carbon nanotubes: Catalytic synthesis and applications. Catal Rev—Sci Eng 2000;42:481–510.
12. Akasaka T, Watari F, Sato Y, Tohji K. Apatite formation on carbon nanotubes. Mat Sci Eng C 2006;26:675–678.
13. Sato Y, Yokoyama A, Shibata KI, Akimoto Y, Ogino SI, Nodasaka Y, Kohgo T, Tamura K, Akasaka T, Uo M, Motomiya K, Jeyadevan B, Ishiguro M, Hataleyama R, Watari F, Tohji K. Influence of length on cytotoxicity of multi-walled carbon nanotubes against human acute monocytic leukemia cell line THP-1 in vitro and subcutaneous tissue of rats in vivo. Molecular BioSyst 2005;1:176–182.
14. Yakoyama A, Sato Y, Nodasaka Y, Yamamoto S, Kawasaki T, Shindoh M, Kohgo M, Akasaka T, Uo M, Watari F, Tohji K. Biological behavior of hat-stacked carbon nanofibers in the subcutaneous tissue in rats. Nano Lett 2005;5:157–161.
15. Elias KL, Price RL, Webster TJ. Enhanced functions of osteoblasts on nanometer diameter carbon fibers. Biomaterials 2002;23: 3279–3287.
16. Ajayan PM.Carbon nanotubes. In: Nalwa HS, editor. Organics, Polymers and Biological Materials, vol. 5. Handbook of Nanostructured Materials and Nanotechnology. San Diego, CA: Academic Press; 2000. pp 375–403.
17. Ebbesen TW. Carbon nanotubes. Phys Today 1996;49:26–32.
18. Yakobson BI, Smalley RE. Fullerene nanotubes: $C_{1,000,000}$ and beyond. Am Sci 1997;85:324–337.
19. Feng F, Meng QC, Zhou Y, Jia D. Spark plasma sintering of functionally graded material in the Ti-TiB2-B system. Mat Sci Eng A 2005;397:92–97.
20. Takechi T, Tabuchi M, Kageyama H, Suyana Y. Prepartion of dense BaTiO3 with submicrometer grains by spark plasma sintering. J Am Ceram Soc 1999;82:939–944.
21. Zhou Y, Hirao K, Toriyama M. Very rapid densification of nanometer silicon electric powder by pulse electric current sintering. J Am Ceram Soc 2000;83:654–657.
22. Nygren M, Shen Z. On the preparation of bio-, nano- and structural ceramics and composites by spark plasma sintering. Solid State Sci 2003;5:125–131.
23. Watari F, Yokoyama A, Omori M, Hirai T, Kondo H, Uo M, Kawasaki T. Biocompatibility of materials and development to functionally graded implant for bio-medical application. Compos Sci Technol 2004;64:893–908.
24. Kondo H, Yokoyama A, Omori M, Ohkubo A, Hirai T, Watari F, Uo M, Kawasaki T. Fabrication of titanium nitride/apatite functionally graded implants by spark plasma sintering. Mater Trans 2004;45:3156–3162.
25. Murakami T, Kitahara A, Koga Y, Kawahara M, Inui H, Yamaguchi M. Microstructure of Nb-Al powders consolidated by spark plasma sintering process. Mater Sci Eng A 1997;239/240:672–679.
26. Yoo S, Groza JR, Sudarshan TS, Yamazaki K. Diffusion bonding of boron nitride on metal substrates by plasma activated sintering (PAS) process. Scripta Mater 1996;34:1383–1386.
27. Groza JR. Consolidation of atomized NiAl powders by plasma activated sintering process. Scripta Metall Mater 1994;30:47–52.
28. Aoki H. Marvelous Biomaterials Apatite. Tokyo, Japan: Ishiyaku Press; 1999.
29. Webster TJ, Ergun C, Doremus RH, Siegel RW, Bizios R. Specific proteins mediate enhanced osteoblast adhesion on nanophase ceramics. J Biomed Mater Res 2000;51:475–483.
30. Webster TJ, Siegel RW, Bizios R. Osteoblast adhesion on nanophase ceramics. Biomaterials 1999;20:1222–1227.

THE JOURNAL OF BONE & JOINT SURGERY (BRITISH)

The responses of extrinsic fibroblasts infiltrating the devitalised patellar tendon to IL-1β are different from those of normal tendon fibroblasts

H. Tohyama,
K. Yasuda,
H. Uchida,
J. Nishihira

From Hokkaido University School of Medicine, Sapporo, Japan

In order to clarify the role of cytokines in the remodelling of the grafted tendon for ligament reconstruction we compared the responses to interleukin (IL)-1β, platelet-derived growth factor (PDGF)-BB and transforming growth factor (TGF)-β1 of extrinsic fibroblasts infiltrating the frozen-thawed patellar tendon in rats with that of the normal tendon fibroblasts, in regard to the gene expression of matrix metalloproteinase (MMP)-13, using Northern blot analysis. We also examined, immunohistologically, the local expression of IL-1β, PDGF-BB, and TGF-β1 in fibroblasts infiltrating the frozen-thawed patellar tendon.

Northern blot analysis showed that fibroblasts derived from the patellar tendon six weeks after the freeze-thaw procedure *in situ* showed less response to IL-1β than normal tendon fibroblasts with respect to MMP-13 mRNA gene expression. The immunohistological findings revealed that IL-1β was over-expressed in extrinsic fibroblasts which infiltrated the patellar tendon two and six weeks after the freeze-thaw procedure *in situ*, but neither PDGF-BB nor TGF-β1 was over-expressed in these extrinsic fibroblasts. Our findings indicated that IL-1β had a close relationship to matrix remodelling of the grafted tendon for ligament reconstruction, in addition to the commencement of inflammation during the tissue-healing process.

H. Tohyama, MD, PhD, Associate Professor
K. Yasuda, MD, PhD, Professor
Department of Sports Medicine
Hokkaido University School of Medicine, Kita-15 Nishi-7, Sapporo, 060-8638, Japan.

H. Uchida, MD, PhD, Assistant Professor
Department of Orthopaedic Surgery, Surgical Science
Tokai University School of Medicine, Bohseidai, Isehara, Kanagawa 259-1193, Japan.

J. Nishihira, MD, PhD, Professor
Department of Medical Information
Hokkaido Information University, Nishi-Nopporo, Ebetsu 069-8585, Japan.

Correspondence should be sent to Dr H. Tohyama; e-mail: tohyama@med.hokudai.ac.jp

doi:10.1302/0301-620X.89B9.18053 $2.00

J Bone Joint Surg [Br] 2007;89-B:1261-7.
Received 24 April 2006; Accepted after revision 21 May 2007

It has been shown that in tendon autografts used for the reconstruction of ligaments, repopulation by fibroblasts from an extrinsic origin occurs during revascularisation after the intrinsic fibroblasts in the tendon have died.[1-3] Numerous studies have shown that various types of cytokine, including interleukin-1 (IL-1), platelet-derived growth factor (PDGF) and transforming growth factor-beta (TGF-β), are over-expressed in fibroblasts in the tissue during healing.[4] These factors are known to regulate the synthesis and degradation of collagen by the fibroblasts.[5,6] It is therefore possible that extrinsic fibroblasts infiltrating necrotised tendons over-express IL-1, PDGF and TGF-β. We have previously observed that extrinsic fibroblasts infiltrating necrotic tendons have significantly different biological characteristics from those of intrinsic fibroblasts in normal tendon as regards proliferation and invasive migration into patellar tendon.[7] There is also a possibility that extrinsic fibroblasts infiltrating the necrotised tendons respond to cytokines differently from the intrinsic fibroblasts in the normal tendon. No studies have compared the responses to cytokines of the two types of fibroblast derived from tendon.

We compared the responses to IL-1β, PDGF-BB, and TGF-β1 of extrinsic fibroblasts infiltrating necrotic patellar tendon and intrinsic fibroblasts in normal tendon as regards the gene expression of matrix metalloproteinase (MMP)-13 using Northern blot analysis, and examined immunohistologically the expression of IL-1β, PDGF-BB, and TGF-β1 in the extrinsic fibroblasts infiltrating the necrotic tendons after freeze-thaw treatment *in situ*.

Materials and Methods

We used 15 male 16-week-old Wistar-King rats with a mean weight of 350 g (330 to 370). In order to compare the responses to IL-1β, PDGF-BB, and TGF-β1 of the extrinsic fibroblasts infiltrating the necrotic patellar tendon and the intrinsic fibroblasts, Northern blot analysis was carried out to evaluate the gene expression of MMP-13 in these two types of fibroblast after stimulation with IL-1β, PDGF-BB or TGF-β1. An immunohistological study examined the local expression of IL-1β, PDGF-BB, and TGF-β1 in the patellar tendon after fibroblast necrosis. All the surgical procedures were carried out in the Institute of Animal Experimentation at Hokkaido University School of Medicine under the Rules and Regulations of the Animal Care and Use Committee.

Experimental design. For Northern blot analysis, we used nine rats. Freeze-thaw treatment was performed *in situ* on the right patellar tendons, while the left knees were left untreated. These rats were killed six weeks later and the patellar tendons harvested. The extrinsic fibroblasts and the normal fibroblasts for Northern blot analysis were obtained from both patellar tendons. The remaining six rats were used for immunohistological evaluation. In these we performed freeze-thaw treatment *in situ* on the right patellar tendon and a sham operation on the left knee. Three were killed at two weeks and the other three at six weeks after surgery, and the patellar tendons on both sides were evaluated immunohistologically.

***In situ* freeze-thaw procedure.** The rats were operated on under sterile conditions and anaesthetised with pentobarbital (50 mg/kg, interperitoneally). The patellar tendon was frozen *in situ* for one minute by liquid nitrogen using a silicone rubber sheet.[8] The frozen tendon was then thawed using physiological saline. Our previous study had shown that there was no cell outgrowth from explants of the tendons which had undergone this freeze-thaw treatment during incubation for two weeks in the culture medium.[8]

Isolation of fibroblasts. After freeze-thaw treatment of the right patellar tendon, each rat was allowed unrestricted activity in its cage. In a previous study, using an identical procedure, we found that fibroblasts were observed in the anterior and posterior parts of the tendon after three to six weeks, while they were widely distributed throughout the thawed tendon at 12 weeks.[8] We therefore selected a time point of six weeks because a number of extrinsic fibroblasts would have infiltrated the necrotic patellar tendon by then and there was a possibility that cellular infiltration would be complete by 12 weeks. For each rat, the extrinsic fibroblasts and the normal fibroblasts were obtained from the right patellar tendon six weeks after freeze-thaw treatment and from the left untreated tendon. The outer synovial layer was removed by sharp dissection and the tendons cut into five pieces, 2 mm to 5 mm in size, and incubated in Dulbecco's modified Eagle's medium (DMEM) containing 10% fetal bovine serum (FBS) at 37°C in a humidified atmosphere of 5% CO_2 and 95% air. A confluent monolayer formed for 14 days or less. When the cells became confluent in the primary tissue-culture dishes, we seeded the cultured fibroblasts from the primary tissue culture into a single 60 mm × 15 mm dish at 10^5 cells at the first passage. They were subcultured at the initial number of 2.5×10^5 cells through the second and third passages. Cells from the third passage were used for all experiments.

Northern blot analysis. To examine the effect of IL-1β, PDGF-BB, and TGF-β1 on the mRNA expression of MMP-13 cultured fibroblasts from the third passage were used throughout the experiment. We used 60 mm × 15 mm dishes for all Northern blot experiments. After reaching confluence, the fibroblasts were rinsed with phosphate-buffered saline, serum-starved for 24 hours, and challenged with recombinant rat IL-1β (R & D Systems, Minneapolis, Minnesota), recombinant human PDGF-BB (R & D Systems) or recombinant human TGF-β1 (R & D Systems) in 10 ml of serum-free DMEM. Northern blot analyses were performed using the templates of rat MMP-13 and glyceraldehyde-3-phosphate dehydrogenase (GAPDH) cDNA which were obtained from a cDNA library (Takara Bio Inc., Ohtu, Japan) of rat synovial fibroblasts. After hybridisation the RNA was transferred on to a nylon membrane, the radioactive bands were then visualised by autoradiography on Kodak X-AR5 film and quantitatively analysed using the NIH Image system (National Institute of Health, Bethseda, Maryland).

Immunohistological examination. The right patellar tendons of six rats underwent freeze-thaw treatment *in situ* to devitalise it,[8] while their left knees had a sham operation. These rats were killed at two and six weeks after the freeze-thaw treatment and both patellar tendons were evaluated immunohistologically. At two or six weeks the rats were perfused transcardially with 100 ml of 10% neutral buffered formalin under anaesthesia. Immunohistochemical staining was performed using Histofine Simple Stain Kit (Rat PO Multi; Nichirei, Tokyo, Japan) with anti-IL-1β antiserum (Yanaihara, Shizuoka, Japan), anti-PDGF-BB polyclonal antibody (Santa Cruz Biotechnology, Santa Cruz, California), and anti-TGF-β monoclonal antibody (Genzyme, Cambridge, Massachussetts).

Statistical analysis. For each Northern blot procedure, all the intensities of the radioactive bands were standardised with respect to those without cytokine stimulation for normal fibroblasts. The relative intensities of MMP-13 to GAPDH were then compared as an internal control between extrinsic and normal tendon fibroblasts using paired *t*-tests at each condition. We also compared the relative intensities of MMP-13 six hours after cytokine stimulation with those without stimulation using paired *t*-tests for each cytokine. The significance limit was set at $p = 0.05$.

Results

Effects of cytokine stimulation on MMP-13 mRNA expression. We carried out Northern blot analysis for the dose dependency and time course using different cell sources. Stimulation with IL-1β and PDGF increased the MMP-13 gene expression of extrinsic fibroblasts depending on the amount of cytokine up to 10 ng/ml and 100 ng/ml respectively, while TGF-β stimulation decreased the MMP-13 gene expression for up to 10 ng/ml (Fig. 1a). The time-course study showed that the MMP-13 gene expression of fibroblasts increased or decreased with time for up to six hours after cytokine stimulation (Fig. 1b). Therefore, we compared the MMP-13 gene expression of extrinsic fibroblasts with that of normal tendon fibroblasts six hours after stimulation with IL-1β of 10 ng/ml, PDGF of 100 ng/ml and TGF-β1 of 10 ng/ml (Fig. 1c).

The relative levels of intensity of MMP-13 mRNA were significantly higher in the extrinsic fibroblasts than in the normal patellar tendon fibroblasts (paired *t*-test, $p = 0.010$;

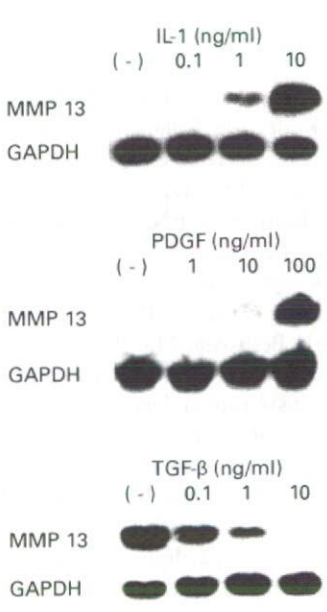

Fig. 1a

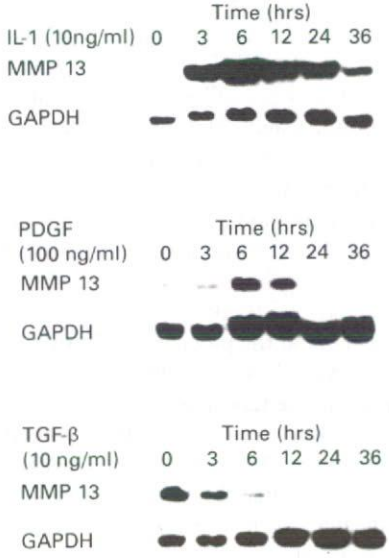

Fig. 1b

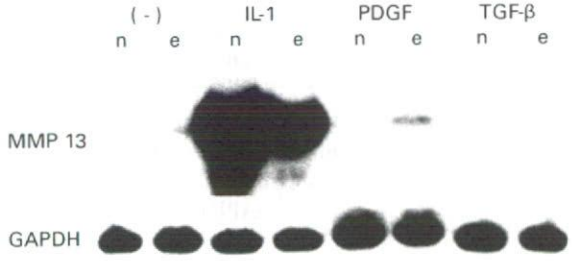

Fig. 1c

Fig. 1 Northern blot analysis of MMP-13 mRNA levels showing a) the effects of the cytokine concentration on MMP-13 mRNA of extrinsic fibroblasts, b) the time course of MMP-13 mRNA of extrinsic fibroblasts after cytokine stimulation and c) the comparison of MMP-13 between normal patellar tendon fibroblasts (n) and extrinsic fibroblasts (e).

Table I). The induction level of MMP-13 mRNA expression by IL-1β stimulation was significantly lower in extrinsic fibroblasts than in the normal patellar tendon fibroblasts (paired *t*-test, p = 0.005), while IL-1β stimulation significantly increased the MMP-13 mRNA expression in both types (paired *t*-test, p = 0.001). Stimulation with PDGF-BB did not have a significant effect on the MMP-13 mRNA expression of either type of fibroblast, while the relative level of MMP-13 mRNA after PDGF-BB stimulation was significantly higher in extrinsic fibroblasts than in the normal tendon fibroblasts (paired *t*-test, p = 0.005). Stimulation with TGF-β1 significantly decreased the MMP-13 mRNA expression in both types of fibroblast. There was no significant difference in MMP-13 mRNA expression after TGF-β1 stimulation in extrinsic and normal fibroblasts (paired *t*-test, p = 0.252).

Local expression of cytokines in extrinsic fibroblasts infiltrating the necrotised tendons. At two weeks after freeze-thaw treatment, no cells were seen in the deep portion of the midsubstance, while cellular infiltration was observed at the superficial portion close to the infrapatellar fat pad (Fig. 2a) and IL-1β-positive cells were found here. At six weeks, a number of fibroblasts were scattered in the tendon and some of these cells expressed IL-1β (Fig. 2b). Tendons with a sham procedure had a minimal amount of staining for IL-1β (Fig 2c and d). Concerning the local expression of PDGF-BB (Fig. 3) and TGF-β (Fig. 4), few positive cells were found in the tendons after the freeze-thaw treatment or the sham operation.